

MINER: MINING THE UNDERLYING PATTERN OF MODALITY-SPECIFIC NEURONS IN MULTIMODAL LARGE LANGUAGE MODELS

Anonymous authors

Paper under double-blind review

ABSTRACT

In recent years, multimodal large language models (MLLMs) have significantly advanced, integrating more modalities into diverse applications. However, the lack of explainability remains a major barrier to their use in scenarios requiring decision transparency. Current neuron-level explanation paradigms mainly focus on knowledge localization or language- and domain-specific analyses, leaving the exploration of multimodality largely unaddressed. To tackle these challenges, we propose **MINER**, a transferable framework for **mining** modality-specific **neurons** (MSNs) in MLLMs, which comprises four stages: **①** modality separation, **②** importance score calculation, **③** importance score aggregation, **④** modality-specific neuron selection. Extensive experiments across six benchmarks and two MLLMs show that **(I)** deactivating **ONLY 2%** of MSNs significantly reduce MLLMs performance (0.56 ~ 0.24 ↓ for Qwen2-VL, 0.69 ~ 0.31 ↓ for Qwen2-Audio), **(II)** different modalities mainly converge in the lower layers, **(III)** MSNs influence how key information from various modalities converges to the last token, **(IV)** We observed two intriguing phenomena, semantic probing and semantic telomers.

1 INTRODUCTION


Recently, multimodal language models (MLLMs) have made rapid advancements across various applications (Xu et al., 2024; Xiao et al., 2024; Yan et al., 2024), exemplified by models like GPT-4 (Achiam et al., 2023), LLaMA 3 (Dubey et al., 2024), Qwen-VL (Bai et al., 2023b), and LLaVA-NEXT (Liu et al., 2024a). However, their

black-box nature presents challenges, particularly in fields like medical studies (González-Alday et al., 2023), where interpretability is essential. Understanding the decision-making process is vital, making explainability a central focus of ongoing research (Tjoa & Guan, 2020; Zhao et al., 2024).

Numerous studies have sought to understand how knowledge is stored in models (Sukhbaatar et al., 2019; Dai et al., 2021; Meng et al., 2022a; Chen et al., 2024a) and how this information influences decision-making (Geva et al., 2020; Petroni et al., 2019). For example, Dai et al. (2021); Geva et al. (2020) investigate knowledge storage mechanisms, while Wendler et al. (2024); Zhang et al. (2024) provide insights into layer-level explainability. Additionally, several works in the neuron-level explanation domain (Tang et al., 2024a; Kojima et al., 2024; Huo et al., 2024) have identified language-specific or domain-specific neurons, referred to as *X-specific neurons*. However, these studies often neglect modality-level understanding, particularly how multimodal information is processed and its differences and similarities (Parekh et al., 2024; Rodis et al., 2023), as shown in table 1.

As shown in table 1 and fig. 1, recent X-specific neuron works (Tang et al., 2024a; Huo et al., 2024) face two key limitations: First, they *focus on sample-level neuron identification*, assuming each sample belongs to a single language or domain, while multimodal samples often span multiple

Table 1: X-specific neuron studies.

		X-SPECIFIC NEURONS		
		Language Tang et al. (2024a)	Domain Huo et al. (2024)	Modality Ours 
GRANULARITY	Sample-level	✓	✓	✗
	Token-level	✗	✗	✓
IMPORTANCE METRICS	Probability	✓	✓	✓
	Mean	✗	✗	✓
	Max	✗	✗	✓
	Attention	✗	✗	✓

054
055
056
057
058
059
060
061
062
063
064
065
066
067
068
069
070
071
072
073
074
075
076
077
078
079
080
081
082
083
084
085
086
087
088
089
090
091
092
093
094
095
096
097
098
099
100
101
102
103
104
105
106
107

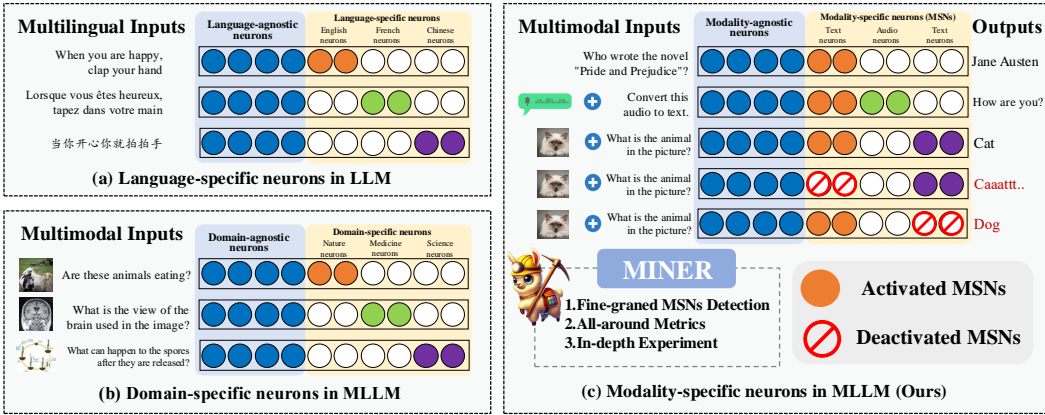


Figure 1: Comparison of Language-specific (a), Domain-specific (b), and our proposed Modality-specific Neuron detection and analysis framework, MINER (c).

modalities. Second, they *rely solely on activation probability as the importance metric*, which is insufficiently comprehensive (See section 4.3 and Ob2 of section 5.4 for details).

This raises an intriguing question: *Are there modality-specific neurons (MSNs) akin to those in multi-language or multi-domain settings?* To address this, we must tackle the following challenges: ❶ How can we measure neuron importance for specific modalities? ❷ What mechanisms do these neurons use to influence the model? ❸ Can we identify some underlying patterns of MSNs?

We propose **MINER**, a transferable framework that develops new importance metrics for measuring neuron significance and introduces selection strategies for identifying key neurons for each modality. MINER tackles the challenges by: ❶ Decompose neuron importance for modalities into token importance from the top down, then restore neuron-modal importance through bottom-up aggregation. ❷ Analyze neuron behavior using feature dimensionality reduction plots and contribution scores of modality tokens to predictions. ❸ Our experiments revealed semantic probing and semantic telomeres. Through this design, we identified a set of important modality-related neurons and uncovered interesting phenomena during our experimental analysis, offering valuable insights for the research community. Our contributions can be summarized as follows:

- ❶ To our knowledge, we are the first to analyze modality-specific neurons (MSNs) in multimodal large language models (MLLMs).
- ❷ We introduce MINER, a transferable framework for selecting MSNs in both vision-based and audio-based MLLMs, capable of handling datasets with any combination of modalities uniformly.
- ❸ We provide a systematic problem definition and propose a novel token-level analysis pipeline that differs from existing sample-level methods.
- ❹ We validate the significance of MSNs through extensive experiments, uncover intriguing phenomena of semantic probing and semantic telomeres, and present new insights.

2 RELATED WORKS

In this section, we provide a brief overview of knowledge location and neuron analysis work, while the related work for the remaining sections is included in appendix B.1.

Knowledge Localization. Research has examined how factual and commonsense knowledge is represented in neural networks (Park et al., 2024; Hase et al., 2024; Zhu et al., 2024). For instance, Sukhbaatar et al. (2019) demonstrated that persistent memory vectors can replace feed-forward network (FFN) layers in transformers without performance loss. Geva et al. (2020) showed that FFN layers serve as key-value memories, linking training patterns to output vocabulary. Recently, Dai et al. (2021) identified *knowledge neurons* in FFN layers of pretrained transformers, positively correlating their activation with factual knowledge expression. Meng et al. (2022a) and Chen et al. (2024a) further explored knowledge neurons in language models. In this context, our analysis aims to identify modality-specific neurons in the FFN layers of MLLMs.

Neuron Analysis. Neuron analysis in pretrained models is an emerging research area in both computer vision and natural language processing. Recent studies have gone beyond explaining the concepts and knowledge represented by individual neurons (Bau et al., 2017; Oikarinen & Weng, 2022; Bills et al., 2023; Gao et al., 2024) to identify neurons that respond to specific patterns. For example, Schubert et al. (2021) and Cammarata et al. (2020) found visual neurons that detect high-frequency features or curves in images, while Tang et al. (2024a) and Kojima et al. (2024) analyzed neurons uniquely activated by target languages, termed *language-specific neurons*, in large language models. In the multimodal domain, research has primarily focused on detecting neurons that respond to both textual and visual inputs (Goh et al., 2021; Schwettmann et al., 2023; Pan et al., 2023). Additionally, Huo et al. (2024) adapted techniques from Tang et al. (2024a) to identify domain-specific neurons (e.g., in medicine and remote sensing) in MLLMs. However, the specialization of neurons in multimodal models is still underexplored. To our knowledge, our work is the **first** to analyze modality-specific neurons in MLLMs.

3 PRELIMINARIES

3.1 DEFINITIONS OF MODALITY, SAMPLE AND DATASET

We start by clarifying two key terms: modality set and modality space, which will be referenced throughout the paper. Building on these definitions, we then define samples and datasets to enhance the understanding of our method.

Modality Set. The classification of modalities in data is not singular. Here, we outline three potential methods for partitioning modality sets:

$$\begin{aligned} S_{\text{all}} &= \{\mathbf{all}\} \\ S_M &= \{\mathbf{text, special, image, video, audio}\} = \{m_1, \dots, m_M\} \\ S_{\text{t+s}} &= \{\mathbf{t+s, image, video, audio}\} \end{aligned}$$

We employ S_M in our method, while S_{all} (treats all as one modality) and $S_{\text{t+s}}$ are used **only** in ablation studies. The **special** modality refers to elements not present in the raw data but introduced by certain MLLMs. For instance, in Qwen2-VL, this includes separators like [im-start] and [im-end] or placeholders such as [image-pad]. The **only** difference between S_M and $S_{\text{t+s}}$ is whether we consider **special** and **text** as the same modality. If treated as the same, we derive $S_{\text{t+s}}$.

Modality Space. Each modality $m \in S_M$ corresponds to a modality space \mathcal{X}_m , encompassing all data or features associated with that modality. This can be formally defined as:

$$\mathcal{X}_m = \{x_m \mid x_m \text{ is a feature corresponding to modality } m_i \text{ from a multimodal sample}\} \quad (1)$$

Additionally, modality space can be viewed as a collection of exclusive information, where data from one space should not overlap with others. For example, the image modality space $\mathcal{X}_{\text{image}}$ includes raw images and features, encompassing all samples related to visual information.

Multimodal Space / Sample. With the foundational definitions of modality established, we define the multimodal sample space as \mathcal{X} , where a sample is represented as:

$$\mathbf{x} = (x_m \mid m \in S_M) \quad \text{where} \quad x_m = \begin{cases} \text{actual modality data} & \text{if modality } m \text{ exists} \\ \text{None} & \text{if modality } m \text{ does not exist} \end{cases}$$

where $x_m \sim \mathcal{X}_m$. For simplicity, we omit $x_m = \text{None}$, allowing a VQA sample to be expressed as $\mathbf{x} = (x_{\text{text}}, x_{\text{image}})$. To perform a fine-grained analysis of multimodal samples, we define the modality function Mod to extract the modality of component x_m as follows:

$$\text{Mod}(x_m) = \begin{cases} m & \text{if } x_m \neq \text{None} \\ \emptyset & \text{otherwise} \end{cases}$$

The modality function can be generalized to extract a sample’s modalities, returning a set of modalities: $\text{Mod}(\mathbf{x}) = \{\text{Mod}(x_m) \mid m \in S_M\}$. For example, $\text{Mod}(\mathbf{x} = (x_{\text{text}}, x_{\text{image}})) = \{\mathbf{text}\}$. We divide the sample space \mathcal{X} into two mutually exclusive subspaces based on the number of modalities: the uni-modality space $\mathcal{X}_{\text{uni}} = \{\mathbf{x} \mid \#\{x_i \mid x_i \neq \text{None}\} = 1\}$ and the multi-modality space $\mathcal{X}_{\text{multi}} = \{\mathbf{x} \mid \#\{x_i \mid x_i \neq \text{None}\} > 1\}$.

Multimodal Dataset. A dataset is a subset of \mathcal{X} where all samples share common characteristics, such as modality or question type. For example, VQA datasets contain both text and image modalities, structured around answering questions. We define uni-modality datasets as $D^{\text{uni}} = \{\mathbf{x}_1, \mathbf{x}_2, \dots \mid \mathbf{x}_i \in \mathcal{X}_{\text{uni}}\}$, and multi-modality datasets as $D^{\text{multi}} = \{\mathbf{x}_1, \mathbf{x}_2, \dots \mid \mathbf{x}_i \in \mathcal{X}_{\text{multi}}\}$.

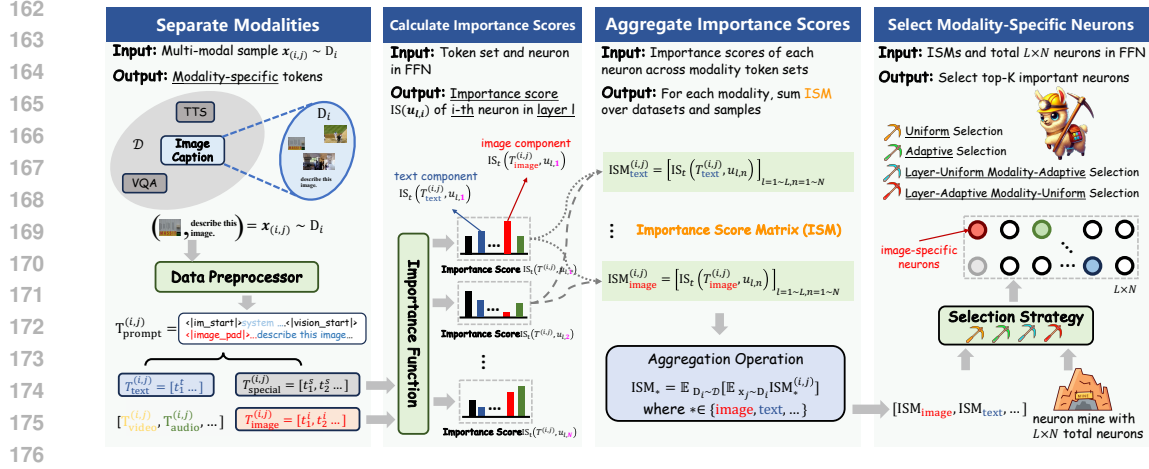


Figure 2: **Four stages of MINER.** ❶ Prompt tokens are divided into modality sets before being input into the LLM. ❷ Each neuron computes an importance score for the tokens of each modality. ❸ Aggregate these values to compute the Importance Score Matrix (ISM), reflecting the modality-level importance of each neuron. ❹ Various selection methods, as detailed in section 4.5, are employed to identify modality-specific neurons for each modality.

3.2 RELEVANT TRANSFORMER CONCEPTS

MLLMs process x using modality-specific encoders and tokenizers (e.g., ViT (Dosovitskiy, 2020a) for **image**), transforming it into a set of **input tokens**:

$$T_{\text{input}} = \bigcup_{m \in S_M} T_m = \{t_1, t_2, \dots, t_I\} \quad \text{where} \quad T_m \cap T_{m'} = \emptyset \quad \text{for} \quad m \neq m' \quad (2)$$

By extending Mod to the token domain, we define $T_m = \{t_i \in T_{\text{input}} | \text{Mod}(t_i) = m\}$ as the modality-specific token set, with size $|T_m| = I_m$. We also establish a mapping structure Ind_m for each subset, enabling retrieval of the original index from the input token set. This allows us to trace any element in T_m back to the original set using the relationship $T_{\text{input}}[\text{Ind}_m[i]] = T_m[i]$.

To enhance clarity in the subsequent definitions, we represent the token embedding corresponding to t_i after being input into the LLM at layer l as $t_i^l \in \mathbb{R}^d$, without distinguishing between the token and its embedding. We denote the embeddings at layer l as $T_{\text{input}}^l = [t_i^l]_{i=1}^I \in \mathbb{R}^{I \times d}$ and the attention matrix after softmax as $\mathbf{A}^l \in \mathbb{R}^{I \times I}$. Ignoring layer normalization, we denote the i -th value vector as v_i^l , allowing us to express the embedding update process as:

$$a_i^l = t_i^l + \sum_{j=1}^I \mathbf{A}_{i,j}^l v_j^l, \quad t_i^{l+1} = a_i^l + W_{\text{out}}^l \text{Act}(W_{\text{in}}^l a_i^l) \quad (3)$$

where $W_{\text{in}} \in \mathbb{R}^{d \times N}$ and $W_{\text{out}} \in \mathbb{R}^{N \times d}$ is the up-sampling and down-sampling layers, respectively. In the equation above, a_i^l represents the output of the attention module, and $\mathbf{H}^l \in \mathbb{R}^{I \times N}$ is the hidden activation vector ($\mathbf{H}_{i,n}^l$ represents the activation value of n -th neuron for token t_i). Each neuron is denoted as $u_{l,n}$, resulting in a total of $L \times N$ neurons in the FFN modules, represented as the matrix $U_{L \times N}$. Then these embeddings pass through L identical transformer blocks, generating output tokens sequentially in an autoregressive manner. We define the set of **output tokens** as $T_{\text{output}} = \{t_{I+1}, t_{I+2}, \dots, t_{I+O}\}$.

4 FRAMEWORK OF MINER

4.1 PROBLEM ANALYSIS

Motivated by previous research on X-specific neurons, such as language-specific Tang et al. (2024a) and domain-specific neurons Huo et al. (2024), our work focuses on identifying a set of MSNs that are *critical for processing multimodal samples in MLLMs*. We briefly analyze how our approach differs from previous studies in fig. 1 and table 1. We focus on neurons in the FFN of MLLMs rather

than other modules, such as modality-specific encoders or projection layers, for several reasons: (I) Previous studies indicate that FFN encode distinct, recoverable knowledge attributes (Geva et al., 2020; Dai et al., 2021; Meng et al., 2022a;b), with some neurons representing the same concepts across different modalities (Schwettmann et al., 2023). (II) Research by Schwettmann et al. (2023) identifies semantic alignment between images and text within the LLM, rather than in the projection layer. (III) Our goal is to identify neurons across modalities within the same set, so we exclude modality-specific encoders. Thus, our research focuses on the FFN module.

Our problem can be distilled into two steps: first, measure a neuron’s importance for a specific modality (Stages 1-3), and second, select the most important neurons based on this measure (Stage 4). Assessing the importance of $u_{l,n}$ in modality space \mathcal{X} is complex due to the infinite number of potential samples. Therefore, we define the **importance score** between a neuron and samples as $IS_s(u_{l,n}, \mathbf{x})$. If a neuron consistently demonstrates importance across many samples, we can conclude it is significant within the modality space. The four stages of MINER align with the sections in fig. 2, outlined as follows:

- ➡ **Stage 1: Modality Separation.** Decomposing the information within the LLM by modality.
- ➡ **Stage 2: Importance Score Calculation.** We decompose the importance of neurons to modalities into their token-level significance and define it accordingly.
- ➡ **Stage 3: Importance Score Aggregation.** We aggregate the token-level importance of neurons to restore their modality-level significance.
- ➡ **Stage 4: Modality-Specific Neuron Selection.** The aggregated scores and a selection strategy are used to identify the top- K important MSNs.

4.2 STAGE 1: MODALITY SEPARATION

To identify neurons associated with specific modalities, we first need to separate the information by modality. While input tokens T_{input} can be divided into distinct sets $\{T_{\text{image}}, T_{\text{text}}, \dots\}$, the attention mechanism blends information across modalities, complicating complete separation. Inspired by the VQA demo in fig. 3, which shows that a small portion of license plate information suffices to answer the question, we propose the following hypothesis:

Hypothesis 1: *As information passes through the LLM layers, most of the content in T_{m_i} remains within its set, with only a small portion related to the question being transferred.*

This hypothesis is supported by confirmatory experiments in section 5.5, prompting us to propose an approximate method for segmenting modality information: we assume the attention module functions only within distinct token sets of different modalities, preventing information exchange between subsets and enabling the partitioning of tokens into mutually exclusive modalities.

Our hypothesis generates a set of uni-modality datasets $\{D_{\text{uni}}^1, D_{\text{uni}}^2, \dots\}$ at the **token level** by partially limiting information flow, aligning to some extent with Tang et al. (2024a); Huo et al. (2024). We further refine the neuron-sample importance function IS_s by defining it at a more granular level between neuron and token set as $IS_t(u_{l,n}, T_m)$. The next stage outlines how we utilize modality information and provides a detailed definition of the importance score.

4.3 STAGE 2: IMPORTANCE SCORE CALCULATION

In the FFN, each neuron outputs an activation value for a token, which naturally serves as an importance score and is widely used (Tang et al., 2024a; Huo et al., 2024). We use $\mathbf{H}_{i,n}^l$, the activation value introduced in section 3.2, as the baseline for all other importance scores (sample-level IS_s , and token-level IS_t). As shown in fig. 12, the significant variation in token counts across modalities makes individual token-based importance unreliable. Therefore, we calculate importance over a token set, removing token count as a factor. We propose the following operations to aggregate activation values for a token set:

- **Prob.** The activation value reflects a neuron’s interest in a token, so we calculate the *interest probability* (activation value > 0) for the tokens:

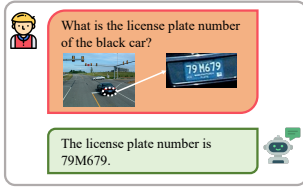


Figure 3: A VQA demo.

$$\text{IS}_t^{\text{Prob}}(u_{l,n}, T_m) = \text{IS}_t^{\text{Prob}}(\mathbf{H}_{1,n}^l, \dots, \mathbf{H}_{I_m,n}^l) = \frac{1}{I_m} \sum_{i=1}^{I_m} \mathbb{I}(\mathbf{H}_{i,n}^l > 0) \quad (4)$$

Here, \mathbb{I} is the indicator function. A higher probability suggests greater engagement with the token set. However, high activation probability doesn't necessarily imply importance. A neuron may have frequent low activations, while fewer high values could indicate a greater contribution. These limitations are confirmed in section 5.4).

- **Mean.** Taking the average is a common approach that captures the group's overall characteristics while balancing the influence of individual tokens. We define this operation as follows:

$$\text{IS}_t^{\text{Mean}}(u_{l,n}, T_m) = \text{IS}_t^{\text{Mean}}(\mathbf{H}_{1,n}^l, \dots, \mathbf{H}_{I_m,n}^l) = \frac{1}{I_m} \sum_{i=1}^{I_m} \mathbf{H}_{i,n}^l \quad (5)$$

- **Max.** We use the maximum activation value as an importance measure. Unlike $\text{IS}_t^{\text{Mean}}$, which represents a uniform distribution, IS_t^{Max} corresponds to a Dirac distribution.
- **Attn-Q.** We developed a method that uses attention values to assess a neuron's importance for a token set, considering each $t_i \in T_{\text{input}}$:

$$\text{IS}_t(u_{l,n}, T_m) = \frac{1}{T} \sum_{i=1}^T \sum_{j=1}^{I_m} w_j(t_i) \mathbf{H}_{\text{Ind}_m[j],n}^l \quad (6)$$

We use Ind_m to map the index of T_m back to T_{input} , retrieving the corresponding values from \mathbf{H} . The $\text{IS}_t^{\text{Attn-Q}}$ employs the i -th row of the attention matrix \mathbf{A} , reflecting the attention scores for the i -th query across all keys, where $\mathbf{w}(t_i) = [w_j(t_i)]_{j=1}^{I_m} = \text{softmax}[\mathbf{A}_{i, \text{Ind}_m[j]}]_{j=1}^{I_m}$.

- **Attn-K.** Like $\text{IS}_t^{\text{Attn-Q}}$, $\text{IS}_t^{\text{Attn-K}}$ uses the i -th column of the attention matrix, reflecting the attention scores for the i -th key across all queries, where $\mathbf{w}(t_i) = \text{softmax}[\mathbf{A}_{\text{Ind}_m[j],i}]_{j=1}^{I_m}$.

As shown in table 1, previous studies on X-specific neuron analysis (Tang et al., 2024a; Huo et al., 2024) rely solely on IS^{Prob} , which has inherent limitations. To address this, we define IS_t as the weighted sum of the five metrics discussed earlier, combining both local and global perspectives. We also evaluate the effectiveness of each metric in section 5.4.

4.4 STAGE 3: IMPORTANCE SCORE AGGREGATION

We calculated the importance score for each neuron across all modality-specific token sets. Next, we aggregate these scores to define the sample-level importance score:

$$\text{IS}_s(u_{l,n}, \mathbf{x}) = \text{IS}_s(u_{l,n}, T_{\text{input}}) = [\text{IS}_t(u_{l,n}, T_m)]_{m \in S_M} \in \mathbb{R}^M \quad (7)$$

For each neuron, we compute a vector as described above, resulting in a sample-level Importance Score Matrix (ISM) defined as $\text{ISM}_s(\mathbf{x}) = [\text{IS}_s(u_{l,n}, \mathbf{x})]_{L,N} \in \mathbb{R}^{M \times L \times N}$. We then aggregate the importance scores across samples from different datasets to obtain the modality-level ISM:

$$\text{ISM}(\mathcal{X}) = \sum_i \sum_j^{|D_i^{\text{multi}}|} \text{ISM}_s(\mathbf{x}_{i,j}) \in \mathbb{R}^{M \times L \times N}, \text{ where } \mathbf{x}_{i,j} \text{ is the } j\text{-th sample of } D_i^{\text{multi}} \quad (8)$$

As the sample size grows, the importance matrix becomes more effective in assessing neuron significance across the entire modality space.

4.5 STAGE 4: MODALITY-SPECIFIC NEURON SELECTION

The previous stage's $\text{ISM}(\mathcal{X})$ evaluates the importance of all neurons in the MLLMs for each modality. We then designed four strategies to select the K highest importance scores from the ISM matrix. However, because of potential neuron overlap, the final number of selected neurons may be less than K . The strategies are implemented as follows:

- (I) **Uniform** selects $\lfloor \frac{K}{L \times M} \rfloor$ neurons for each modality in every layer (the strongest assumption).
- (II) **LA-MU** (Layer-Adaptive & Modality-Uniform) selects $\lfloor \frac{K}{M} \rfloor$ neurons for each modality, allowing for adaptive quantities in each layer and relaxing certain constraints.
- (III) **LU-MA** (Layer-Uniform & Modality-Adaptive) selects $\lfloor \frac{K}{L} \rfloor$ neurons for each layer.
- (IV) **Adaptive** selects K positions in the ISM matrix without constraints on modality or layer.

fig. 4 intuitively illustrates the segmentation methods for the four selection strategies. The assumptions range from strong to weak, beginning with a fixed number of neurons for each modality in every layer and progressively relaxing constraints until the fourth approach imposes no limitations. Together, these strategies offer a comprehensive set of selection criteria.

Using any selection strategy, we generate neuron positions as a Boolean mask $\mathbf{B} \in \{0, 1\}^{L \times N}$ (with 1 indicating MSNs). As shown in eq. (8), different datasets yield distinct ISM, resulting in varied masks. Thus, with all other settings fixed, a specific dataset combination uniquely determines a neuron mask. For simplicity, we can define a mask function as $\mathbf{B} = \text{mask}(D_1, D_2, \dots)$.

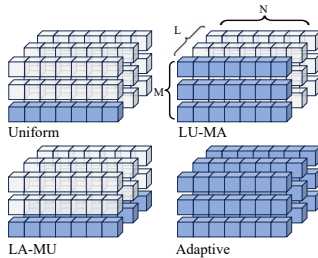


Figure 4: Selection strategies.

5 EXPERIMENT

We apply MINER in various settings to explore the existence and characteristics of MSNs. Our study aims to answer the following research questions:

- ✦ RQ1: Do the identified modality-specific neurons significantly contribute to multimodal models?
- ✦ RQ2: If RQ1 is validated, how do these neurons facilitate this contribution?
- ✦ RQ3: How do different hyperparameter settings influence the behavior of the MLLMs?
- ✦ RQ4: Can we uncover underlying patterns among modality-specific neurons?

5.1 EXPERIMENT SETUP

Unless otherwise noted (e.g., in ablation studies), we adopt the following default settings. We define S_M as the modality set, treating **special** and **text** as distinct modalities. We deactivate neurons across **all modalities** by setting their outputs to zero, then evaluate the impact on performance.

Models. We select Qwen2-VL (Wang et al., 2024) for visual tasks and Qwen2-Audio (Chu et al., 2024) for audio tasks to ensure a thorough exploration of the current model landscape. Qwen2-VL processes text, image, and video modalities, while Qwen2-Audio focuses on text and audio.

Datasets. For text-only tasks, we chose MMLU (Hendrycks et al., 2020). For text-image tasks, we selected TextVQA (Singh et al., 2019), and for text-video tasks, we opted for MSVD-QA (Chen & Dolan, 2011). Since no datasets exist for image-only or audio-only tasks, we selected specific datasets with fixed prompts to minimize the impact of the text modality. For an approximate image-only dataset, we utilized the MS-COCO 2014 captioning benchmark (Lin et al., 2014), adopting the Karpathy split test set as per Li et al. (2023); Tang et al. (2024b); Zhan et al. (2024) by fixing the text tokens. For an approximate audio-only dataset, we employed LibriSpeech (Panayotov et al., 2015) and VocalSound (Gong et al., 2022) in a similar manner.

5.2 MAIN RESULTS (RQ1)

To address RQ1, we generate neuron masks for each dataset combination to thoroughly evaluate our method. The main results for Qwen2-VL and Qwen2-Audio are shown in table 2 and table 3. Key experimental observations (Obs) include:

Ob1. Masking just 2% of neurons impacts performance. The first row in both tables shows normal inference without masking. After masking the selected neurons, we

observe performance drops, except for a slight increase in MSVD (analyzed later). Results in table 4 show that randomly masking 2% of neurons has no effect, confirming that the modality-specific neurons identified by our method significantly influence model performance.

Table 3: **Qwen2-Audio results:** Same format as table 2.

DATASETS			QWEN2-AUDIO (0.69 ~ 0.31 ↓)			
			MMLU	LibriSpeech	VocalSound	Average
MMLU	Libri	Vocal	Accuracy	WRR	Accuracy	
-	-	-	0.40	0.94	0.74	0.69
✓			0.00	0.53	0.41	0.31
	✓		0.01	0.85	0.15	0.34
		✓	0.01	0.87	0.19	0.36
✓	✓		0.00	0.85	0.34	0.40
✓		✓	0.01	0.86	0.37	0.39
	✓	✓	0.01	0.81	0.35	0.39
✓	✓	✓	0.01	0.83	0.40	0.41

Table 2: **Main results of Qwen2-VL.** We select MSNs (2%) using various dataset combinations (indicated by \checkmark) and then mask neurons across all modalities, recording the performance of the masked MLLMs. The minimum value in each column is marked in blue. We highlight any new values in gray when adding a new dataset improves the mask’s quality.

DATASETS				QWEN2-VL (0.56 ~ 0.24 ↓)						
TextVQA	COCO Caption	MMLU	MSVD-QA	TextVQA Accuracy	COCO Caption			MMLU Accuracy	MSVD-QA Accuracy	Average
				Accuracy	BLEU	S-BERT	CIDEr	Accuracy	Accuracy	
-	-	-	-	0.90	0.10	0.79	0.36	0.69	0.51	0.56
\checkmark				0.75	0.04	0.18	0.10	0.57	0.52	0.36
	\checkmark			0.80	0.01	0.14	0.18	0.52	0.53	0.36
		\checkmark		0.87	0.03	0.70	0.34	0.59	0.50	0.51
			\checkmark	0.38	0.01	0.14	0.18	0.44	0.32	0.25
\checkmark	\checkmark			0.77	0.04	0.28	0.16	0.55	0.54	0.39
\checkmark		\checkmark		0.79	0.03	0.19	0.14	0.56	0.46	0.36
\checkmark			\checkmark	0.78	0.05	0.33	0.20	0.57	0.54	0.41
	\checkmark	\checkmark		0.79	0.02	0.41	0.27	0.50	0.45	0.41
	\checkmark		\checkmark	0.85	0.10	0.61	0.34	0.59	0.52	0.50
		\checkmark	\checkmark	0.40	0.01	0.15	0.17	0.41	0.31	0.24
\checkmark	\checkmark	\checkmark		0.76	0.04	0.49	0.30	0.53	0.45	0.43
\checkmark	\checkmark		\checkmark	0.82	0.06	0.39	0.26	0.60	0.42	0.43
\checkmark		\checkmark	\checkmark	0.78	0.04	0.35	0.24	0.57	0.48	0.41
	\checkmark	\checkmark	\checkmark	0.84	0.05	0.61	0.33	0.58	0.48	0.48
\checkmark	\checkmark	\checkmark	\checkmark	0.82	0.06	0.53	0.29	0.56	0.52	0.46

Ob2. Neurons identified from diverse datasets are higher quality. For MSVD-QA performance, apply mask(MSVD) drops performance to 0.32, while apply mask(MSVD, COCO) raises it to 0.52. This may be because the diverse text questions in MSVD-QA closely relate to video semantics, producing high-quality text-specific neurons. In contrast, the fixed text prompts in COCO Caption (see fig. 7) create a repetitive pattern, degrading neuron mask quality. MMLU’s diverse text data causes a larger performance drop (0.31) when combined with MSVD-QA.

Ob3. Adding more datasets can improve MSNs quality. Many values in both tables are highlighted in Gray, showing that new datasets often enhance mask quality. However, some cases also demonstrate decreased effectiveness, possibly due to the diversity issues mentioned in Ob3 or conflicts among dataset characteristics that lead to incompatible ISM matrices. We will investigate these phenomena in future work.

5.3 NEURON FUNCTIONALITY PRINCIPLES (RQ2)

This research question focuses on the intrinsic mechanisms of action of MSNs. Several key observations are as follows:

Ob1. The audio modality exhibits a “semantic probing” effect towards the text modality, indicating a potential trend toward aligning key information across modalities. We present the feature distribution under three masking settings in fig. 5-(a). The complementary mask is defined as $1 - \mathbf{B}$. As the layer depth increases, audio embeddings extend “tentacles” toward the embeddings of other modalities, a phenomenon we call “semantic probing.” This suggests that the LLM aligns not the entire modal feature space, but specific key information.

Ob2. A “semantic telomeres” phenomenon occurs in special modality, anchoring at the edges of the text modality’s semantic space. In fig. 5-(a), text embeddings initially form circular clusters that elongate into strips in deeper layers. Special tokens progressively align with and stabilize at the front of these clusters, a pattern we refer to as “semantic telomeres.”

Ob3. MSNs shape MLLMs behavior by directing how key information from different modality tokens converges into the last token. We apply mask(COCO) to the COCO Caption dataset and calculate each modality’s contribution score to the final prediction based on the accumulated attention between its token set and the last token. As shown in fig. 5-(b), applying a mask for a specific modality results in $\Delta < 0$, indicating reduced information flow to the last token.

5.4 ABLATION STUDIES (RQ3)

We present ablation studies on MINER’s components and highlight key observations:

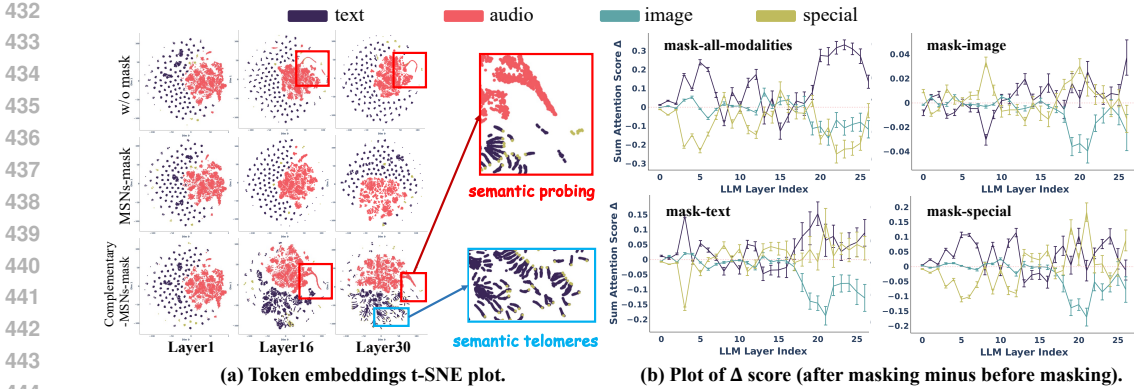


Figure 5: (a) t-SNE plots for VocalSound, showcasing three masking settings: no masking, Mask(VocalSound), and complementary masking (from top to bottom). (b) Display the change (Δ) in contribution scores between different token sets and the last token before and after masking, based on 100 samples (detail in section 5.3).

Ob1. Selection strategies with appropriate degrees of freedom yield higher-quality MSNs. As shown in table 4, the uniform method, which imposes a fixed number of neurons per modality at each layer, performed the worst. In contrast, greater flexibility in selecting neurons across modalities and layers enabled a better approximation of important neuron distribution. Among these strategies, LA-MU proved most effective, as it maintained flexibility in neuron counts across layers while treating all modalities equally, thus avoiding imbalances.

Ob2. For the importance metrics, the activation probability was less effective than our other designs.

We evaluated the effectiveness of each of the five importance metrics individually and also assessed the impact of combining them. As shown in table 4, the activation probability performed poorly, aligning with the section 4.3 analysis. In contrast, our newly designed metrics, which account for both local and global perspectives, demonstrate improved effectiveness.

Table 4: **Ablation results.** Red (blue) indicates the minimum in each row (column), and green highlights values that are minimum in both.

IMPORTANCE METRIC					SELECTION STRATEGY				
Prob	Mean	Max	A-K	A-Q	Uniform	LU-MA	LA-MU	Adaptive	Random
1					0.88	0.88	0.89	0.88	0.90
	1				0.87	0.87	0.85	0.89	0.89
		1			0.81	0.66	0.83	0.85	0.90
			1		0.87	0.87	0.85	0.89	0.90
				1	0.87	0.88	0.85	0.89	0.90
	1/2	1/2			0.83	0.82	0.81	0.17	0.90
			1/2	1/2	0.87	0.88	0.85	0.89	0.90
	1/4	1/4	1/2		0.84	0.85	0.76	0.84	0.90
	1/4	1/4		1/2	0.85	0.85	0.81	0.80	0.90
1/5	1/5	1/5	1/5	1/5	0.86	0.87	0.89	0.90	0.90

Ob3. The model’s performance significantly drops with an increase in masked MSNs. As shown in fig. 6-(a), masking 1% of neurons has minimal impact, while 5% nearly collapses performance. Therefore, MINER selects 2% to strike a balance.

Ob4. The model’s performance is greatly influenced by the deactivation value settings. Considering neuron $u_{l,n}$, we test three deactivation settings: fixing its output activation to 0, -0.1, and $\min(\mathbf{H}^l)$. As shown in fig. 6-(a), a slightly negative activation value reduces model performance, indirectly highlighting the importance of the identified neurons for the modality, since randomly deactivated neurons below zero do not impact performance.

Ob5. Considering “special” and “text” as separate modalities leads to improved results. We evaluate three modality sets: S_{all} , S_M and S_{t+s} defined in section 3.1, referred to as “all”, “t,s”, and “t+s” in fig. 6-(a). The poor performance of S_{all} shows that our sample-level issue (all in one modality) cannot be resolved, highlighting the need for modality separation at the token level.

Ob6. Masking MSNs from different modalities affects performance, with a greater impact as more modalities are masked. We apply mask(COCO) to the COCO Caption dataset and normalize values within different metrics to a 0-1 range. Results are shown in Figure 1, with “t,” “s,” and “i” representing text, special, and image, respectively. We found that performance declines significantly with an increasing number of masked modalities.

486
487
488
489
490
491
492
493
494
495
496
497
498
499
500
501
502
503
504
505
506
507
508
509
510
511
512
513
514
515
516
517
518
519
520
521
522
523
524
525
526
527
528
529
530
531
532
533
534
535
536
537
538
539

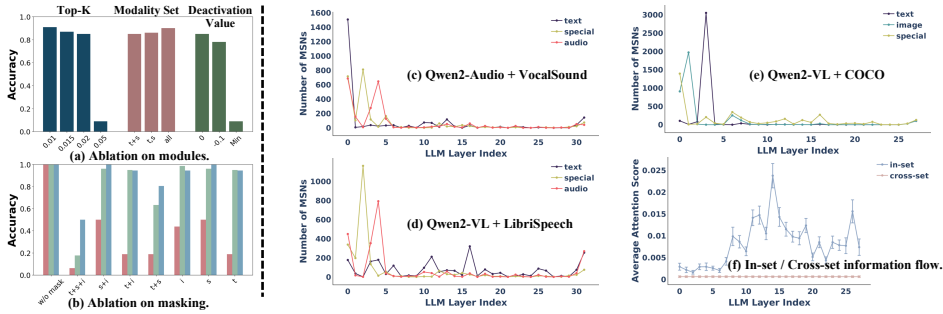


Figure 6: (a) and (b) present the ablation results, while (c), (d), and (e) illustrate the neuron distribution across layers. (f) shows the information flow within and between token sets.

5.5 IDENTIFYING PATTERNS IN NEURONS (RQ4)

In this section, we investigate potential MSNs patterns through experiments to offer valuable insights. Our key observations are as follows:

Ob1. Most MSNs are concentrated in the shallow layers, with only a small portion in the final layers. As shown in fig. 6, figures (c), (d), and (e) visualize the distribution of modality-specific neurons across layers. This trend aligns with findings in Zhang et al. (2024), indicating that cross-modal perception primarily occurs in the early layers (detailed in appendix B.2). Thus, we believe that different modalities primarily converge in the lower layers.

Ob2. Most modality information stays within the token set, with only a small amount of key information transferring to other sets. To validate Hypothesis 1 from section 4.2, we measure information flow using attention values, calculating the cumulative in-set attention and cross-set attention (the diagonal blocks of A). We apply mask(MSVD-QA) to the MSVD-QA dataset, with results shown in fig. 6-(f). Our findings indicate that in-set information flow significantly surpasses cross-set flow, supporting our hypothesis.

6 CONCLUSION

To our knowledge, this is the **first** study of modality-specific neurons (MSNs) in MLLMs. We select a small set of key neurons from the FFN that are crucial for processing multimodal data and design experiments to investigate their underlying mechanisms. We address this issue through the following steps: ❶ Define key concepts related to modalities, samples, and datasets. ❷ Conduct sample-level and token-level analyses to differentiate modality information at a finer granularity, evaluate the limitations of existing importance metrics, and propose new ones. ❸ Calculate importance scores for neurons associated with a set of tokens and aggregate these scores across samples and datasets for a global modality-level analysis. ❹ Define four selection strategies to extract the top-*K* neurons with the highest importance scores as the output MSNs. In the experimental section, we validate our method by masking the MSNs and observing the resulting decline in model performance, while also identifying two intriguing phenomena: semantic probing and semantic telomers.

6.1 LIMITATION AND FUTURE WORK

Our work presents several areas for improvement: (I) We introduced the independence hypothesis of token sets to separate information by modality; however, key information exchanges between token sets occur and are difficult to capture. Future research could relax this assumption by incorporating cross-set information exchange for potentially better results. (II) Our study focused on vision-related Qwen2-VL and audio-related Qwen2-Audio models, limiting the range of modalities. Future work aims to include broader MLLMs, such as any-to-any models, and datasets with more diverse modalities. (III) We observed two intriguing phenomena—semantic probing and semantic telomers—whose underlying causes remain unclear, presenting an opportunity for further exploration. (IV) The quality of datasets directly influences the quality of identified neurons, which may be linked to data diversity. Future research could investigate this further and design metrics to quantify dataset quality. (V) While this work emphasizes identifying important neurons, the next step is to explore how to leverage these neurons to enhance MLLMs performance on relevant modalities, potentially through neuron fine-tuning techniques.

REFERENCES

- 540
541
542 Josh Achiam, Steven Adler, Sandhini Agarwal, Lama Ahmad, Ilge Akkaya, Florencia Leoni Ale-
543 man, Diogo Almeida, Janko Altenschmidt, Sam Altman, Shyamal Anadkat, et al. Gpt-4 technical
544 report. *arXiv preprint arXiv:2303.08774*, 2023.
- 545
546 Jinze Bai, Shuai Bai, Yunfei Chu, Zeyu Cui, Kai Dang, Xiaodong Deng, Yang Fan, Wenbin Ge,
547 Yu Han, Fei Huang, et al. Qwen technical report. *arXiv preprint arXiv:2309.16609*, 2023a.
- 548
549 Jinze Bai, Shuai Bai, Shusheng Yang, Shijie Wang, Sinan Tan, Peng Wang, Junyang Lin, Chang
550 Zhou, and Jingren Zhou. Qwen-vl: A versatile vision-language model for understanding, local-
551 ization, text reading, and beyond. *arXiv preprint arXiv:2308.12966*, 2023b.
- 552
553 David Bau, Bolei Zhou, Aditya Khosla, Aude Oliva, and Antonio Torralba. Network dissection:
554 Quantifying interpretability of deep visual representations. In *Proceedings of the IEEE conference*
555 *on computer vision and pattern recognition*, pp. 6541–6549, 2017.
- 556
557 Steven Bills, Nick Cammarata, Dan Mossing, Henk Tillman, Leo Gao, Gabriel Goh, Ilya Sutskever,
558 Jan Leike, Jeff Wu, and William Saunders. Language models can explain neurons in lan-
559 guage models. URL [https://openaipublic.blob.core.windows.net/neuron-explainer/paper/index.](https://openaipublic.blob.core.windows.net/neuron-explainer/paper/index.html)
560 *html*.(Date accessed: 14.05. 2023), 2, 2023.
- 561
562 Nick Cammarata, Gabriel Goh, Shan Carter, Ludwig Schubert, Michael Petrov, and Chris Olah.
563 Curve detectors. *Distill*, 5(6):e00024–003, 2020.
- 564
565 David Chen and William B Dolan. Collecting highly parallel data for paraphrase evaluation. In
566 *Proceedings of the 49th annual meeting of the association for computational linguistics: human*
567 *language technologies*, pp. 190–200, 2011.
- 568
569 Yuheng Chen, Pengfei Cao, Yubo Chen, Kang Liu, and Jun Zhao. Journey to the center of the
570 knowledge neurons: Discoveries of language-independent knowledge neurons and degenerate
571 knowledge neurons. In *Proceedings of the AAAI Conference on Artificial Intelligence*, volume 38,
572 pp. 17817–17825, 2024a.
- 573
574 Zhe Chen, Jiannan Wu, Wenhai Wang, Weijie Su, Guo Chen, Sen Xing, Muyan Zhong, Qinglong
575 Zhang, Xizhou Zhu, Lewei Lu, et al. Internvl: Scaling up vision foundation models and aligning
576 for generic visual-linguistic tasks. In *Proceedings of the IEEE/CVF Conference on Computer*
577 *Vision and Pattern Recognition*, pp. 24185–24198, 2024b.
- 578
579 Yunfei Chu, Jin Xu, Xiaohuan Zhou, Qian Yang, Shiliang Zhang, Zhijie Yan, Chang Zhou, and
580 Jingren Zhou. Qwen-audio: Advancing universal audio understanding via unified large-scale
581 audio-language models. *arXiv preprint arXiv:2311.07919*, 2023.
- 582
583 Yunfei Chu, Jin Xu, Qian Yang, Haojie Wei, Xipin Wei, Zhifang Guo, Yichong Leng, Yuanjun Lv,
584 Jinzheng He, Junyang Lin, et al. Qwen2-audio technical report. *arXiv preprint arXiv:2407.10759*,
585 2024.
- 586
587 Damai Dai, Li Dong, Yaru Hao, Zhifang Sui, Baobao Chang, and Furu Wei. Knowledge neurons in
588 pretrained transformers. *arXiv preprint arXiv:2104.08696*, 2021.
- 589
590 Nilaksh Das, Saket Dingliwal, Srikanth Ronanki, Rohit Paturi, David Huang, Prashant Mathur, Jie
591 Yuan, Dhanush Bekal, Xing Niu, Sai Muralidhar Jayanthi, et al. Speechverse: A large-scale
592 generalizable audio language model. *arXiv preprint arXiv:2405.08295*, 2024.
- 593
594 Soham Deshmukh, Benjamin Elizalde, Rita Singh, and Huaming Wang. Pengi: An audio language
595 model for audio tasks. *Advances in Neural Information Processing Systems*, 36:18090–18108,
596 2023.
- 597
598 Alexey Dosovitskiy. An image is worth 16x16 words: Transformers for image recognition at scale.
599 *arXiv preprint arXiv:2010.11929*, 2020a.
- 600
601 Alexey Dosovitskiy. An image is worth 16x16 words: Transformers for image recognition at scale.
602 *arXiv preprint arXiv:2010.11929*, 2020b.

- 594 Abhimanyu Dubey, Abhinav Jauhri, Abhinav Pandey, Abhishek Kadian, Ahmad Al-Dahle, Aiesha
595 Letman, Akhil Mathur, Alan Schelten, Amy Yang, Angela Fan, et al. The llama 3 herd of models.
596 *arXiv preprint arXiv:2407.21783*, 2024.
597
- 598 Leo Gao, Tom Dupré la Tour, Henk Tillman, Gabriel Goh, Rajan Troll, Alec Radford, Ilya
599 Sutskever, Jan Leike, and Jeffrey Wu. Scaling and evaluating sparse autoencoders. *arXiv preprint*
600 *arXiv:2406.04093*, 2024.
- 601 Mor Geva, Roei Schuster, Jonathan Berant, and Omer Levy. Transformer feed-forward layers are
602 key-value memories. *arXiv preprint arXiv:2012.14913*, 2020.
603
- 604 Gabriel Goh, Nick Cammarata, Chelsea Voss, Shan Carter, Michael Petrov, Ludwig Schubert, Alec
605 Radford, and Chris Olah. Multimodal neurons in artificial neural networks. *Distill*, 6(3):e30,
606 2021.
- 607 Yuan Gong, Jin Yu, and James Glass. Vocalsound: A dataset for improving human vocal sounds
608 recognition. In *ICASSP 2022-2022 IEEE International Conference on Acoustics, Speech and*
609 *Signal Processing (ICASSP)*, pp. 151–155. IEEE, 2022.
610
- 611 Raquel González-Alday, Esteban García-Cuesta, Casimir A Kulikowski, and Victor Maojo. A
612 scoping review on the progress, applicability, and future of explainable artificial intelligence in
613 medicine. *Applied Sciences*, 13(19):10778, 2023.
614
- 615 Peter Hase, Mohit Bansal, Been Kim, and Asma Ghandeharioun. Does localization inform editing?
616 surprising differences in causality-based localization vs. knowledge editing in language models.
617 *Advances in Neural Information Processing Systems*, 36, 2024.
- 618 Dan Hendrycks, Collin Burns, Steven Basart, Andy Zou, Mantas Mazeika, Dawn Song, and
619 Jacob Steinhardt. Measuring massive multitask language understanding. *arXiv preprint*
620 *arXiv:2009.03300*, 2020.
621
- 622 Jiahao Huo, Yibo Yan, Boren Hu, Yutao Yue, and Xuming Hu. Mmneuron: Discovering
623 neuron-level domain-specific interpretation in multimodal large language model. *arXiv preprint*
624 *arXiv:2406.11193*, 2024.
- 625 Takeshi Kojima, Itsuki Okimura, Yusuke Iwasawa, Hitomi Yanaka, and Yutaka Matsuo. On
626 the multilingual ability of decoder-based pre-trained language models: Finding and control-
627 ling language-specific neurons. In Kevin Duh, Helena Gomez, and Steven Bethard (eds.),
628 *Proceedings of the 2024 Conference of the North American Chapter of the Association for*
629 *Computational Linguistics: Human Language Technologies (Volume 1: Long Papers)*, pp.
630 6919–6971, Mexico City, Mexico, June 2024. Association for Computational Linguistics. doi:
631 10.18653/v1/2024.naacl-long.384.
- 632 Junnan Li, Dongxu Li, Silvio Savarese, and Steven Hoi. Blip-2: Bootstrapping language-image
633 pre-training with frozen image encoders and large language models. In *International conference*
634 *on machine learning*, pp. 19730–19742. PMLR, 2023.
635
- 636 Tsung-Yi Lin, Michael Maire, Serge Belongie, James Hays, Pietro Perona, Deva Ramanan, Piotr
637 Dollár, and C Lawrence Zitnick. Microsoft coco: Common objects in context. In *Computer*
638 *Vision—ECCV 2014: 13th European Conference, Zurich, Switzerland, September 6–12, 2014,*
639 *Proceedings, Part V 13*, pp. 740–755. Springer, 2014.
640
- 641 Haotian Liu, Chunyuan Li, Yuheng Li, Bo Li, Yuanhan Zhang, Sheng Shen, and Yong Jae Lee.
642 Llava-next: Improved reasoning, ocr, and world knowledge, January 2024a.
- 643 Haotian Liu, Chunyuan Li, Qingyang Wu, and Yong Jae Lee. Visual instruction tuning. *Advances*
644 *in neural information processing systems*, 36, 2024b.
645
- 646 Yuan Liu, Haodong Duan, Yuanhan Zhang, Bo Li, Songyang Zhang, Wangbo Zhao, Yike Yuan,
647 Jiaqi Wang, Conghui He, Ziwei Liu, et al. Mmbench: Is your multi-modal model an all-around
player? *arXiv preprint arXiv:2307.06281*, 2023.

- 648 Haoyu Lu, Wen Liu, Bo Zhang, Bingxuan Wang, Kai Dong, Bo Liu, Jingxiang Sun, Tongzheng Ren,
649 Zhuoshu Li, Yaofeng Sun, et al. Deepseek-vl: towards real-world vision-language understanding.
650 *arXiv preprint arXiv:2403.05525*, 2024.
- 651
- 652 Kevin Meng, David Bau, Alex Andonian, and Yonatan Belinkov. Locating and editing factual asso-
653 ciations in gpt. *Advances in Neural Information Processing Systems*, 35:17359–17372, 2022a.
- 654
- 655 Kevin Meng, Arnab Sen Sharma, Alex Andonian, Yonatan Belinkov, and David Bau. Mass-editing
656 memory in a transformer. *arXiv preprint arXiv:2210.07229*, 2022b.
- 657
- 658 Tuomas Oikarinen and Tsui-Wei Weng. Clip-dissect: Automatic description of neuron representa-
659 tions in deep vision networks. *arXiv preprint arXiv:2204.10965*, 2022.
- 660
- 661 Haowen Pan, Yixin Cao, Xiaozhi Wang, and Xun Yang. Finding and editing multi-modal neurons
662 in pre-trained transformer. *arXiv preprint arXiv:2311.07470*, 2023.
- 663
- 664 Vassil Panayotov, Guoguo Chen, Daniel Povey, and Sanjeev Khudanpur. Librispeech: an asr corpus
665 based on public domain audio books. In *2015 IEEE international conference on acoustics, speech*
666 *and signal processing (ICASSP)*, pp. 5206–5210. IEEE, 2015.
- 667
- 668 Jayneel Parekh, Pegah Khayatan, Mustafa Shukor, Alasdair Newson, and Matthieu Cord. A concept-
669 based explainability framework for large multimodal models. *arXiv preprint arXiv:2406.08074*,
670 2024.
- 671
- 672 Jae Sung Park, Jack Hessel, Khyathi Chandu, Paul Pu Liang, Ximing Lu, Peter West, Youngjae Yu,
673 Qiuyuan Huang, Jianfeng Gao, Ali Farhadi, et al. Localized symbolic knowledge distillation for
674 visual commonsense models. *Advances in Neural Information Processing Systems*, 36, 2024.
- 675
- 676 Fabio Petroni, Tim Rocktäschel, Patrick Lewis, Anton Bakhtin, Yuxiang Wu, Alexander H Miller,
677 and Sebastian Riedel. Language models as knowledge bases? *arXiv preprint arXiv:1909.01066*,
678 2019.
- 679
- 680 Alec Radford, Jong Wook Kim, Tao Xu, Greg Brockman, Christine McLeavey, and Ilya Sutskever.
681 Robust speech recognition via large-scale weak supervision, 2022.
- 682
- 683 Nikolaos Rodis, Christos Sardanios, Georgios Th Papadopoulos, Panagiotis Radoglou-Grammatikis,
684 Panagiotis Sarigiannidis, and Iraklis Varlamis. Multimodal explainable artificial intelligence: A
685 comprehensive review of methodological advances and future research directions. *arXiv preprint*
686 *arXiv:2306.05731*, 2023.
- 687
- 688 Ludwig Schubert, Chelsea Voss, Nick Cammarata, Gabriel Goh, and Chris Olah. High-low fre-
689 quency detectors. *Distill*, 6(1):e00024–005, 2021.
- 690
- 691 Sarah Schwettmann, Neil Chowdhury, Samuel Klein, David Bau, and Antonio Torralba. Multimodal
692 neurons in pretrained text-only transformers. In *Proceedings of the IEEE/CVF International Con-*
693 *ference on Computer Vision*, pp. 2862–2867, 2023.
- 694
- 695 Amanpreet Singh, Vivek Natarajan, Meet Shah, Yu Jiang, Xinlei Chen, Dhruv Batra, Devi Parikh,
696 and Marcus Rohrbach. Towards vqa models that can read. In *Proceedings of the IEEE/CVF*
697 *conference on computer vision and pattern recognition*, pp. 8317–8326, 2019.
- 698
- 699 Sainbayar Sukhbaatar, Edouard Grave, Guillaume Lample, Herve Jegou, and Armand Joulin. Aug-
700 menting self-attention with persistent memory. *arXiv preprint arXiv:1907.01470*, 2019.
- 701
- 702 Changli Tang, Wenyi Yu, Guangzhi Sun, Xianzhao Chen, Tian Tan, Wei Li, Lu Lu, Zejun Ma,
703 and Chao Zhang. Salmonn: Towards generic hearing abilities for large language models. *arXiv*
704 *preprint arXiv:2310.13289*, 2023.
- 705
- 706 Tianyi Tang, Wenyang Luo, Haoyang Huang, Dongdong Zhang, Xiaolei Wang, Xin Zhao, Furu
707 Wei, and Ji-Rong Wen. Language-specific neurons: The key to multilingual capabilities in large
708 language models. In Lun-Wei Ku, Andre Martins, and Vivek Srikumar (eds.), *Proceedings of the*
709 *62nd Annual Meeting of the Association for Computational Linguistics (Volume 1: Long Papers)*,
710 pp. 5701–5715, Bangkok, Thailand, August 2024a. Association for Computational Linguistics.

- 702 Zineng Tang, Ziyi Yang, Chenguang Zhu, Michael Zeng, and Mohit Bansal. Any-to-any generation
703 via composable diffusion. *Advances in Neural Information Processing Systems*, 36, 2024b.
704
- 705 Erico Tjoa and Cuntai Guan. A survey on explainable artificial intelligence (xai): Toward medical
706 xai. *IEEE transactions on neural networks and learning systems*, 32(11):4793–4813, 2020.
- 707 Peng Wang, Shuai Bai, Sinan Tan, Shijie Wang, Zhihao Fan, Jinze Bai, Keqin Chen, Xuejing Liu,
708 Jialin Wang, Wenbin Ge, et al. Qwen2-vl: Enhancing vision-language model’s perception of the
709 world at any resolution. *arXiv preprint arXiv:2409.12191*, 2024.
- 710
- 711 Chris Wendler, Veniamin Veselovsky, Giovanni Monea, and Robert West. Do llamas work in en-
712 glish? on the latent language of multilingual transformers. *arXiv preprint arXiv:2402.10588*,
713 2024.
- 714 Jian Wu, Yashesh Gaur, Zhuo Chen, Long Zhou, Yimeng Zhu, Tianrui Wang, Jinyu Li, Shujie Liu,
715 Bo Ren, Linqun Liu, et al. On decoder-only architecture for speech-to-text and large language
716 model integration. In *2023 IEEE Automatic Speech Recognition and Understanding Workshop*
717 *(ASRU)*, pp. 1–8. IEEE, 2023.
- 718
- 719 Hanguang Xiao, Feizhong Zhou, Xingyue Liu, Tianqi Liu, Zhipeng Li, Xin Liu, and Xiaoxuan
720 Huang. A comprehensive survey of large language models and multimodal large language models
721 in medicine. *arXiv preprint arXiv:2405.08603*, 2024.
- 722
- 723 Baixuan Xu, Weiqi Wang, Haochen Shi, Wenxuan Ding, Huihao Jing, Tianqing Fang, Jiaxin
724 Bai, Long Chen, and Yangqiu Song. Mind: Multimodal shopping intention distillation
725 from large vision-language models for e-commerce purchase understanding. *arXiv preprint*
arXiv:2406.10701, 2024.
- 726
- 727 Yibo Yan, Haomin Wen, Siru Zhong, Wei Chen, Haodong Chen, Qingsong Wen, Roger Zimmer-
728 mann, and Yuxuan Liang. Urbanclip: Learning text-enhanced urban region profiling with con-
729 trastive language-image pretraining from the web. In *Proceedings of the ACM on Web Conference*
2024, pp. 4006–4017, 2024.
- 730
- 731 An Yang, Baosong Yang, Binyuan Hui, Bo Zheng, Bowen Yu, Chang Zhou, Chengpeng Li,
732 Chengyuan Li, Dayiheng Liu, Fei Huang, et al. Qwen2 technical report. *arXiv preprint*
arXiv:2407.10671, 2024.
- 733
- 734 Jun Zhan, Junqi Dai, Jiasheng Ye, Yunhua Zhou, Dong Zhang, Zhigeng Liu, Xin Zhang, Ruibin
735 Yuan, Ge Zhang, Linyang Li, et al. Anygpt: Unified multimodal llm with discrete sequence
736 modeling. *arXiv preprint arXiv:2402.12226*, 2024.
- 737
- 738 Xiaofeng Zhang, Chen Shen, Xiaosong Yuan, Shaotian Yan, Liang Xie, Wenxiao Wang, Chaochen
739 Gu, Hao Tang, and Jieping Ye. From redundancy to relevance: Enhancing explainability in mul-
740 timodal large language models. *arXiv preprint arXiv:2406.06579*, 2024.
- 741
- 742 Haiyan Zhao, Hanjie Chen, Fan Yang, Ninghao Liu, Huiqi Deng, Hengyi Cai, Shuaiqiang Wang,
743 Dawei Yin, and Mengnan Du. Explainability for large language models: A survey. *ACM Trans-*
actions on Intelligent Systems and Technology, 15(2):1–38, 2024.
- 744
- 745 Deyao Zhu, Jun Chen, Xiaoqian Shen, Xiang Li, and Mohamed Elhoseiny. Minigpt-4: En-
746 hancing vision-language understanding with advanced large language models. *arXiv preprint*
arXiv:2304.10592, 2023.
- 747
- 748 Junyi Zhu, Shuo Chen Liu, Yu Yu, Bo Tang, Yibo Yan, Zhiyu Li, Feiyu Xiong, Tong Xu, and
749 Matthew B Blaschko. Fastmem: Fast memorization of prompt improves context awareness of
750 large language models. *arXiv preprint arXiv:2406.16069*, 2024.
- 751
- 752
- 753
- 754
- 755

A DATASET DETAILS

This section presents a detailed description of the datasets used in our evaluation, including data samples and the prompts provided to MLLMs.

A.1 TEXTVQA

TextVQA (Singh et al., 2019) is a dataset for Visual Question Answering (VQA) that focuses on answering questions about text found in images. It features a variety of images, such as signs and labels, requiring models to combine visual understanding with Optical Character Recognition (OCR) to accurately respond to questions. TextVQA is a key benchmark for evaluating the integration of visual and textual reasoning in AI models.

A.2 COCO CAPTION

The COCO Caption dataset (Lin et al., 2014) is a large-scale resource containing over 1.5 million captions that describe more than 330,000 images, distributed across 80 diverse object categories. The images were selected to represent complex, real-world scenes, depicting everyday environments where common objects appear in their natural contexts. Each image is annotated with five captions, each of which was independently generated by human annotators. COCO Caption dataset has been a foundational benchmark for training and evaluating the image captioning performance of multimodal large language models.

A.3 MMLU

The Massive Multitask Language Understanding (MMLU) (Hendrycks et al., 2020) dataset is a benchmark for evaluating language models across 57 subjects, ranging from elementary topics to advanced academic fields. It consists of multiple-choice questions testing a model’s knowledge and reasoning across diverse domains. MMLU is widely used to assess the generalization capabilities of large language models.

A.4 MSVD-QA

The MSVD (Microsoft Research Video Description Corpus) (Chen & Dolan, 2011), also known as YouTube2Text, consists of 1,970 short videos, each ranging from 10 to 25 seconds with an average duration of 9 seconds. These videos depict a variety of subjects, including people, animals, actions, and different scenes. Each video is annotated with multiple sentences by different annotators, averaging around 41 sentences per clip, resulting in a total of 80,839 sentences. On average, each sentence contains 8 words, with approximately 16,000 unique words across the dataset.

A.5 LIBRISPEECH

LibriSpeech (Panayotov et al., 2015) is a widely used dataset for automatic speech recognition (ASR) tasks. It contains approximately 1,000 hours of 16kHz English speech, sourced from the LibriVox audiobooks. The dataset is divided into several subsets, including “clean” and “other”, which distinguish recordings by noise levels. Each audio file is accompanied by an accurate transcription, making it ideal for training and evaluating ASR models. LibriSpeech’s diverse speaker base and detailed annotations also make it suitable for tasks like speaker identification and voice synthesis.

A.6 VOCALSOUND

VocalSound (Gong et al., 2022) is an open dataset containing 21,024 crowdsourced recordings of human vocalizations such as laughter, sighs, coughs, throat clearing, sneezes, and sniffing, from 3,365 individuals. Designed for classification tasks, it enables models to accurately identify various non-speech sounds. The dataset also includes metadata like speaker age, gender, native language, country, and health status, supporting research on how demographic factors affect vocal sounds.

810 With its comprehensive scope and detailed annotations, VocalSound is a valuable resource for im-
811 proving models in human vocalization classification.
812

813 A.7 PROMPTS OF DATASETS 814

815
816 Generate a caption for the image in one short sentence, similar to these examples from the
817 COCO dataset:

- 818 1. A man with a red helmet on a small moped on a dirt road.
- 819 2. Man riding a motor bike on a dirt road on the countryside.
- 820 3. A man riding on the back of a motorcycle.
- 821 4. A man in a red shirt and a red hat is on a motorcycle on a hill side.

822 Now, describe the image.
823
824

825 Figure 7: Prompt for COCO Caption.
826
827

828 The following are multiple choice questions (with answers) about abstract algebra.
829

830 Find all c in Z_3 such that $Z_3[x]/(x^2 + c)$ is a field.

831 **A.** 0

832 **B.** 1

833 **C.** 2

834 **D.** 3

835 **Answer:** B

836 ...

837 Find the degree for the given field extension $Q(\sqrt{2}, \sqrt{3}, \sqrt{18})$ over Q .

838 **A.** 0

839 **B.** 4

840 **C.** 2

841 **D.** 6

842 **Answer:**
843
844

845 Figure 8: Prompt for MMLU.
846
847

848 Please transcribe the following audio directly into plain text without any additional explana-
849 tions, prefixes, or descriptions.

850 Only output the transcription of the spoken content in the audio.
851
852

853 Figure 9: Prompt for LibriSpeech.
854
855

856 A.8 DATASET SAMPLE STATISTICS 857

858 B ADDITIONAL RESULTS 859

860 B.1 ADDITIONAL RELATED WORKS 861

862 **Development of MLLMs.** Researchers have extensively investigated integrating additional modal-
863 ities into foundational large language models (Liu et al., 2023). Notably, large vision-language mod-
els (Zhu et al., 2023) and audio-language models (Deshmukh et al., 2023) have gained significant

864
865
866
867
868
869
870
871
872
873
874
875
876
877
878
879
880
881
882
883
884
885
886
887
888
889
890
891
892
893
894
895
896
897
898
899
900
901
902
903
904
905
906
907
908
909
910
911
912
913
914
915
916
917

You are a sound classification model. Your task is to classify a given audio sample into one of the following categories based on its content:

1. Laughter
2. Sigh
3. Cough
4. Throat clearing
5. Sneeze
6. Sniff

Please analyze the audio sample and provide the corresponding category name.

Figure 10: Prompt for Vocal Sound.

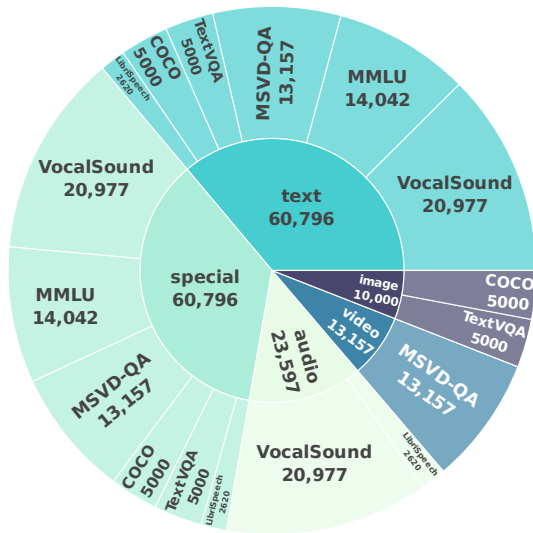


Figure 11: **Sample-level count statistics for different modalities.** We provide a sample-level statistical analysis of all datasets used in this work. The inner ring represents different modalities, while the outer ring corresponds to the respective datasets, with sample counts labeled on both rings. For instance, a VQA sample containing text, special, and image modalities is counted under each modality it includes.

attention by combining visual or audio inputs with text. For instance, (Liu et al., 2024b) proposed aligning images with text by projecting visual embeddings from a pretrained vision encoder into word space through a single MLP layer, allowing LLMs to understand the post-projection tokens. Similarly, Chen et al. (2024b) and Lu et al. (2024) used various projectors for this alignment. Recently, Qwen2-VL (Bai et al., 2023b) introduced a universal vision encoder that processes both images and videos, integrating visual embeddings directly into the textual token stream. Parallely, several studies have focused on integrating audio data into LLMs (Deshmukh et al., 2023; Wu et al., 2023), typically involving post-processing of auditory embeddings through additional modules like Q-Former (Tang et al., 2023) or downsampling layers (Das et al., 2024). Notably, Qwen2-Audio (Chu et al., 2023) has surpassed previous state-of-the-art models across various audio benchmarks without task-specific fine-tuning. In this research, we selected Qwen2-VL and Qwen2-Audio as our vision-language and audio-language baselines, both utilizing Qwen-7B (Bai et al., 2023a; Yang et al., 2024) as the foundational LLM, with Vision Transformer (Dosovitskiy, 2020b) and Whisper-large-v3 (Radford et al., 2022) serving as their respective vision and audio encoders.

B.2 ALL DISTRIBUTIONS OF NEURONS ACROSS LAYERS

918
919
920
921
922
923
924
925
926
927
928
929
930
931
932
933
934
935
936
937
938
939
940
941
942
943
944
945
946
947
948
949
950
951
952
953
954
955
956
957
958
959
960
961
962
963
964
965
966
967
968
969
970
971

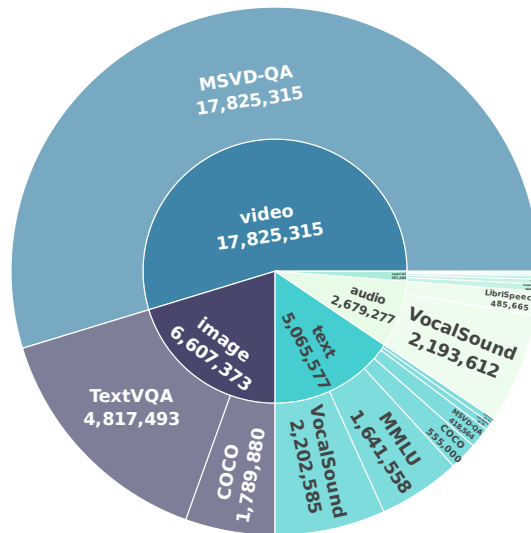


Figure 12: **Token-level count statistics for different modalities.** This image provides a token-level analysis. The inner ring represents different modalities, while the outer ring shows the corresponding datasets. We process each sample’s modality components through specific encoders and tokenizers to generate token sets, which are then categorized and summarized in the pie chart. Although the number of samples across datasets is balanced, the token count varies significantly by modality—video encoding produces far more tokens than text encoding, for instance. This underscores the need to compute importance scores within each modality’s token set and normalize by token count for fair cross-modality comparisons.

972
973
974
975
976
977
978
979
980
981
982
983
984
985
986
987
988
989
990
991
992
993
994
995
996
997
998
999
1000
1001
1002
1003
1004
1005
1006
1007
1008
1009
1010
1011
1012
1013
1014
1015
1016
1017
1018
1019
1020
1021
1022
1023
1024
1025

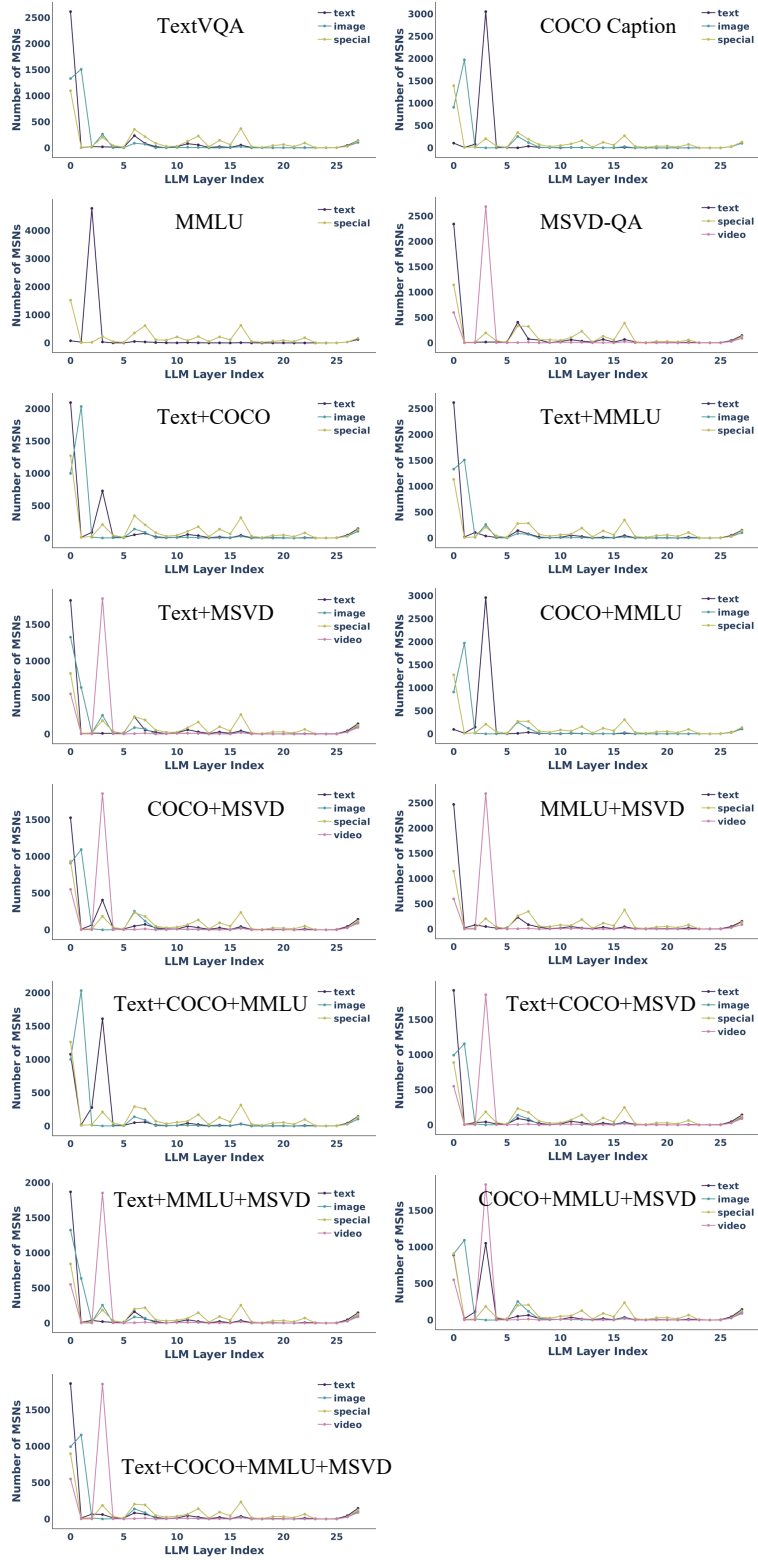


Figure 13: The distribution of modality-specific neurons across different layers, derived from all possible dataset combinations in Qwen2-VL.

1026
 1027
 1028
 1029
 1030
 1031
 1032
 1033
 1034
 1035
 1036
 1037
 1038
 1039
 1040
 1041
 1042
 1043
 1044
 1045
 1046
 1047
 1048
 1049
 1050
 1051
 1052
 1053
 1054
 1055
 1056
 1057
 1058
 1059
 1060
 1061
 1062
 1063
 1064
 1065
 1066
 1067
 1068
 1069
 1070
 1071
 1072
 1073
 1074
 1075
 1076
 1077
 1078
 1079

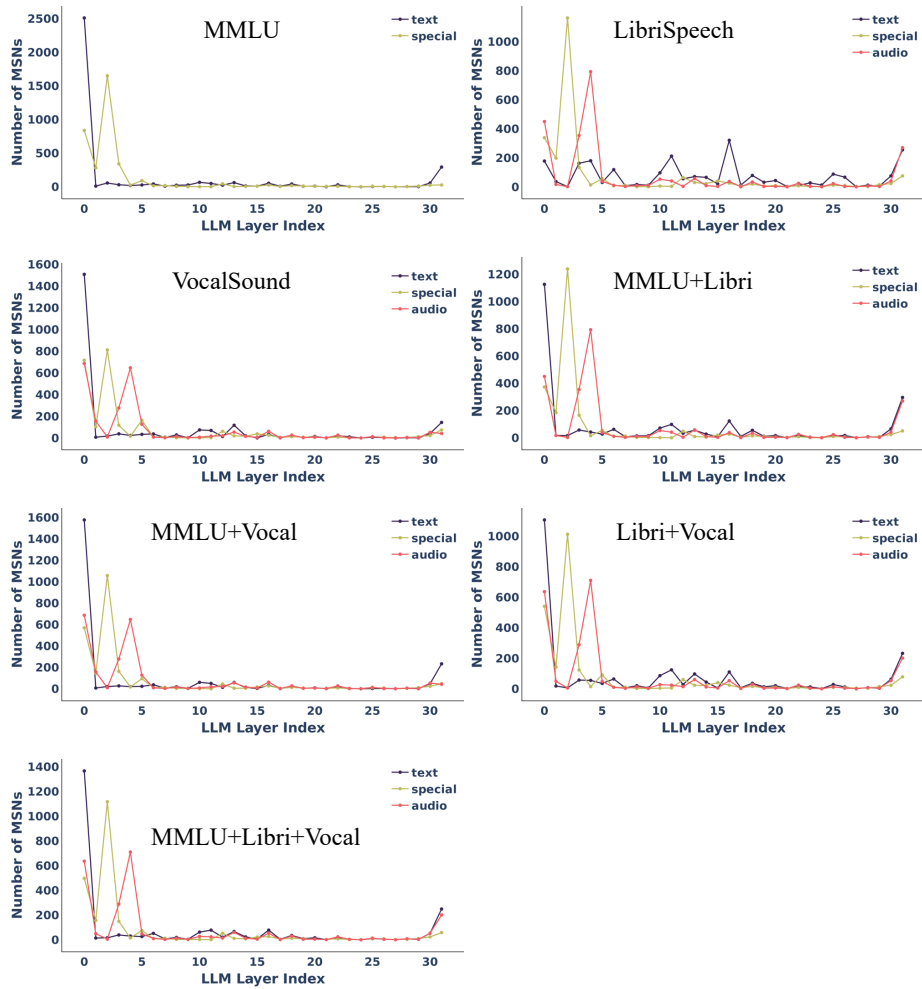


Figure 14: The distribution of modality-specific neurons across different layers, derived from all possible dataset combinations in Qwen2-Audio.